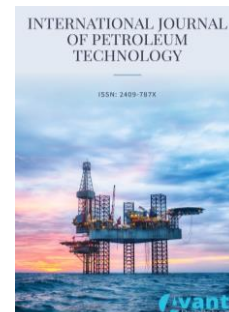




Published by Avanti Publishers
**International Journal of Petroleum
Technology**
ISSN (online): 2409-787X




Experimental Measurements to Study Correlations between Porosity, Absolute Permeability, and Capillary Pressure

Walid M. Mahmud * and Adel M. Jaluta

Department of Petroleum Engineering, University of Tripoli, Tripoli, Libya

ARTICLE INFO

Article Type: Research Article

Academic Editor: Murtada Elhaj 

Keywords:

Tortuosity

Porosity-permeability correlations

Permeability-capillary pressure relationship

Timeline:

Received: May 13, 2023

Accepted: August 24, 2023

Published: September 22, 2023

Citation: Mahmud WM, Jaluta AM. Experimental measurements to study correlations between porosity, absolute permeability, and capillary pressure. Int J Petrol Technol. 2023; 10: 71-80.

DOI: <https://doi.org/10.15377/2409-787X.2023.10.6>

ABSTRACT

Rock permeability is a measurement of how easily a fluid can flow through a rock while porosity is a measure of the rock's storage capacity or its pore volume that is capable of holding fluids. In many cases correlations may exist between porosity and permeability, however, these correlations are usually derived for a certain formation, and therefore they do not exhibit general application or validity. Cross-plot of permeability versus porosity data, to create a porosity-permeability transform, is sometimes used to assign permeability values to areas of a reservoir where permeability data are unavailable. The capillary pressure curve is also used to predict rock absolute permeability. In the present work, porosity, absolute permeability, and capillary pressure were measured experimentally to investigate and establish new correlations between porosity, Klinkenberg-corrected permeability, and capillary pressure. Fifty-nine core plugs, obtained from two different fields located in Sirte basin, Libya, were utilized. Results indicate that porosity might be a reasonable estimator of permeability, as correlations between porosity and permeability were observed and empirical permeability equations based on porosity were established. Capillary pressure was observed to be overall inversely proportional to permeability, however, determined capillary pressure curves varied within the same formation.

*Corresponding Author

Email: w.mahmud@uot.edu.ly

Tel: +(218) 091 323 0494

©2023 Mahmud and Jaluta. Published by Avanti Publishers. This is an open access article licensed under the terms of the Creative Commons Attribution Non-Commercial License which permits unrestricted, non-commercial use, distribution and reproduction in any medium, provided the work is properly cited. (<http://creativecommons.org/licenses/by-nc/4.0/>)

1. Introduction

Correlations between porosity and permeability have been extensively investigated and numerous reservoir characterization studies utilized the relationship between porosity and permeability whenever it existed. Two different rocks may have identical porosity but two entirely different permeabilities and vice versa. Porosity and tortuosity, among other interconnected porous media physical properties, are utilized to express permeability [1, 2]. Detailed knowledge of pore and throat size distributions and spatial arrangement of the pore channels within the rock is necessary to link permeability with porosity [3]. Establishing a relationship or correlation between important reservoir parameters such as porosity and permeability is crucial for understanding fluid flow in porous media. Detmer [4] studied correlations between porosity and permeability on outcrop sediments and observed weak correlation between porosity and permeability concluding that porosity was not a good estimator of permeability. Berg [5] and Bloch [6] attempted to establish a relationship between porosity and permeability. However, conflicting trends were observed between porosity and permeability. The Kozeny-Carman (KC) relationship is a widely utilized technique of relating porosity to permeability. The technique is simple and effective first proposed by Kozeny [7] and subsequently modified by Carman [8]. However, such simplicity, of the technique, can be a limiting factor that rock grains are considered spherical and packed in a regular arrangement indicating that pore bodies are becoming capillary bundles. This may lead to exaggerated permeabilities in many heterogeneous, tortuous, complex, or poorly connected reservoir rocks [9]. Moreover, permeability can be strongly dependent on the direction of flow while porosity is a global property. Thus, correlations between porosity and permeability may be observable, however, they are strongly dependent on pore structure [10]. Establishing correlations between rock petrophysical properties and capillary pressure curves requires that a mathematical model fit the capillary pressure curves. Thus, several methods have been proposed to estimate permeability from capillary pressure curves [10-20]. For instance, mercury capillary pressure was empirically utilized to obtain permeability from the graphical integral of the mercury saturation curve versus reciprocal capillary pressure squared [10]. Thomeer [21] utilized a log-log plot of capillary pressure data and developed a mathematical expression for permeability. He empirically related the hyperbolic functions to permeability. Swanson [12] introduced new correlations between capillary pressure curve and permeability, that avoided capillary pressure curve lower plateau, and introduced an effective porosity or saturation that contributes most to fluid flow. Dullien [22], Serra [23], Pittman [24], and Rezaee and Lemon [25] also utilized capillary pressure to estimate permeability. Niya and Selvadurai [1] performed numerical simulations to establish statistical correlations between permeability, porosity, tortuosity, and conductance. Mahmud [3] conducted rate-controlled mercury injection experiments and obtained three distinct capillary pressure curves that can be utilized to estimate permeability. Permeability is proportional to the square of pore throat size; therefore, permeability increases with the increase of larger connected pore throats. Pore throats are represented by threshold entry capillary pressures that may be very high for very tight rocks and shales where the effective throat radius is very small. Whereas threshold capillary pressure may be very small for vuggy limestone consisting of large pores as well as for sandstones in which some particles are microporous such as clay or chert particles, and also for fractured rocks. Cut-off is another criterion that limits values of particular parameters such as porosity and permeability [26]. Reservoir quality is greatly affected by reservoir grain sizes as the reservoir quality increases with porosity and permeability increase. The porosity-permeability relationship is the most traditional tool for determining porosity cut-off [27]. Pore throat radius and porosity are frequently used to calculate permeability using multivariate statistical analysis. The shape of capillary pressure curves, which relate to the volume of pore space controlled by pore throats of a given size, also affect permeability. Pore throat distribution controls the number of macro and micro pore throats and their associated pore volume that are accessed and occupied by the non-wetting phase at different saturation ranges. Porosity, on the other hand, is directly proportional to mainly the volume of pore bodies and less extent the volume of throats [3]. Well testing is used to measure permeability, however, core analysis under reservoir or ambient conditions is a common method for direct measurements of porosity and permeability.

In this study, experimental data regression analysis was used to predict permeability from porosity and develop new correlations between porosity, Klinkenberg-corrected permeability, and capillary pressure for sandstone rocks. Results obtained confirm the presence of correlations between porosity and permeability. Data

utilized were based on experimental analysis on cores obtained from two wells located in two different sandstone oil fields located in Sirte basin, Libya. This study also briefly discusses the evaluation of permeability from capillary pressure curves.

2. Experimental Procedures and Data Analysis

Two full-diameter cores from wells A and B with lengths of 30 and 28 feet were utilized to obtain small core plugs to be used to accomplish the objectives of the present study. As previously indicated, wells A and B are located in two different oil fields in Sirte basin, Libya. A total of 59 core plugs were considered. The core plugs exhibit a wide range of porosity and permeability as shown in Fig. (1-4).

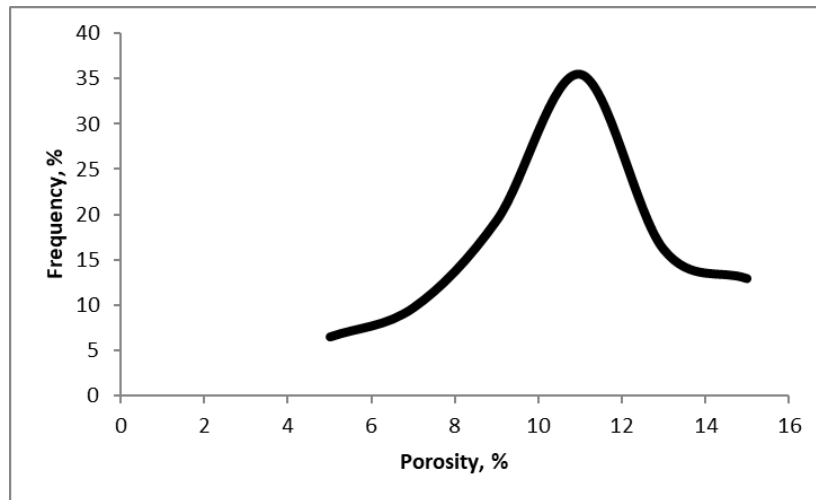


Figure 1: Porosity frequency distribution of core plugs obtained from well A.

A Helium Porosimeter was utilized to measure the porosity of selected core plugs at ambient conditions. The method measures pore volume yielding effective porosity.

Liquid and gas permeability can be determined on core plugs in the laboratory; however, it is usually more convenient to measure permeability in the laboratory using a gas as the working fluid. Liquids may adsorb onto the rock surface and potentially change wettability which could adversely affect later experiments. Utilizing gas does not affect wettability, core plug preparation is simple and the analytical procedure is fairly rapid. A gas permeameter was used to measure the absolute permeability of the core plugs. The instrument has been specifically designed to allow quick and easy loading and unloading of core plugs.

2.1. Core Plug Preparation

A diamond core bit was used with water as the bit coolant and lubricant to drill through the one-and-a-half-inch diameter core plugs of the two wells. A total of 31 core plugs were dissected from the full-diameter core of well A and 28 core plugs were dissected from the full-diameter core of well B. Hydrocarbons were extracted from the core plugs using toluene and methanol was used to leach the core plugs of salt. Core plugs were then dried in an oven at 80 °C. Potential additional salts in the pore spaces were removed by Silver Nitrate solution. Finally, core plugs were tested for hydrocarbon presence utilizing fluorescence under ultraviolet. Table 1 illustrates visual observations assessed on the core plugs. The effective porosity and permeability of the core plugs ranged from 4.14 to 32.64 percent and from 0.515 mD to 140.37 mD, respectively.

Fig. (1 and 2) show porosity and permeability frequencies, respectively, of core plugs obtained from well A. From Fig. (1), most core plugs of well A, have porosities of around 35% and from Fig. (2), most core plugs, have permeabilities of around 15 mD.

Table 1: Visual observations on the 59 core plugs.

Well A		Well B	
Core Plug #	Observations	Core Plug #	Observations
1	Fractures	32	Intact
2	Fractures	33	Intact
3	Fractures	34	Intact
4	Fractures	35	Vugs
5	Fractures	36	Intact
6	Intact	37	Intact
7	Fractures	38	Intact
8	Fractures	39	Intact
9	Intact	40	Intact
10	Intact	41	Intact
11	Fractures	42	Intact
12	Fractures & Vugs	43	Intact
13	Fractures	44	Intact
14	Intact	45	Intact
15	Intact	46	Intact
16	Intact	47	Intact
17	Fractures	48	Intact
18	Fractures	49	Intact
19	Fractures	50	Intact
20	Broken Edge	51	Intact
21	Fractures	52	Intact
22	Intact	53	Intact
23	Fractures	54	Intact
24	Intact	55	Intact
25	Fractures & Vugs	56	Intact
26	Fractures	57	Intact
27	Fractures	58	Intact
28	Fractures	59	Vugs
29	Fractures	-	-
30	Fractures	-	-
31	Intact	-	-

Fig. (3 and 4) show porosity and permeability frequencies, respectively, of core plugs obtained from well B. From Fig. (3), most core plugs of well B, have porosities of around 27% and from Fig. (4), most core plugs, have permeabilities of around 8 mD. Porosity ranges from 4.14 to 15.94% with an average of 10.73% and from 23.8 to 32.64% with an average of 27.23% for the core plugs from wells A and B, respectively. Permeability ranges from 0.515 to 140.37 mD and from 1.3 to 24.1 mD for the core plugs of wells A and B, respectively. Pore throat radius

distribution of all core plugs ranges from 0.174 to 20.87 μm with an average of 5.2 μm . The core plugs exhibit a wide range in pore throat radius as pore types were nanopores and micropores [3].

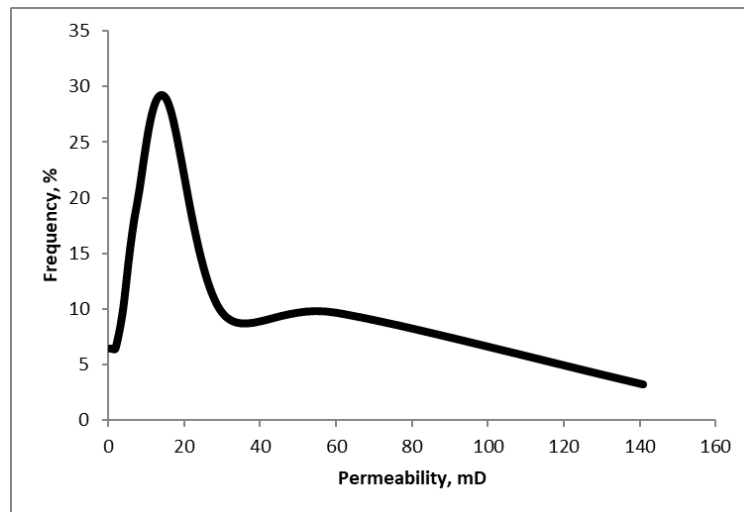


Figure 2: Permeability frequency distribution of core plugs obtained from well A.

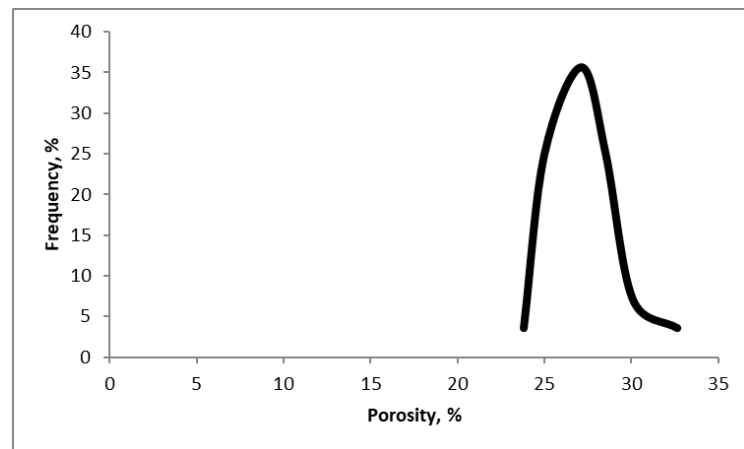


Figure 3: Porosity frequency distribution of core plugs obtained from well B.

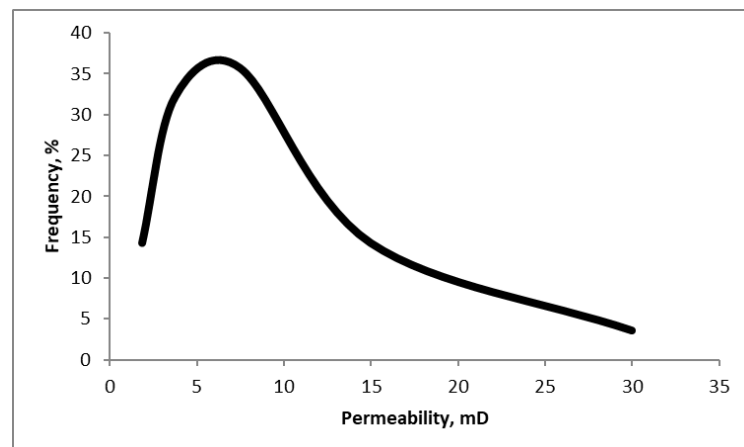


Figure 4: Permeability frequency distribution of core plugs obtained from well B.

2.2. Helium Gas Expansion Porosimeter

A helium expansion gas porosimeter with a twin cell was used for measuring grain volume of the core plugs. The principle used in the porosimeter to measure porosity is Boyle's law. Helium gas was placed at ambient temperature in the instrument at a sealed reference chamber to a pressure of 100 psig. Then cores were placed in a different chamber that is sealed and linked by a two-way valve to the reference chamber. The valve, whenever unlocked, permits gas expansion from the reference chamber to the two chambers' total volume. Thus, by knowing the initial and final pressures as well as the volume of the reference chamber and by utilizing Boyle's Law, volume of the chamber containing the core plug can be established. Calibration of the instrument was performed before utilizing the porosimeter. Stainless steel blanks that have known volumes were run, for calibration, so that jointly with the reciprocal of the final pressure a graph of the blank volume can be plotted. The plot was then input into linear regression software that yields an equation for core plug grain volume and culminating pressure reading. From the bulk volume and weight calculations, grain density and porosity can be determined. The instrument has a pressure indicator with a remote pressure transducer range of 0-100 psi, resolution of 0.01 psi, and accuracy of + 0.1% of the entire scale. The Precision Pressure Controller of the instrument has a range of 0-100 psi at resolution and repeatability better than 0.01 and 0.02 psi, respectively.

2.3. Positive Displacement Pump

Bulk volume of core plugs was calculated by a positive displacement mercury pump which is a stainless steel high-pressure pycnometer that contains the core plug connected to a volumetric pump cylinder. Mercury is supplied or withdrawn from the core plug chamber whenever the hand wheel attached to the pump is wound in or out. The pressure transducer attached to the pump digitally measures mercury volume. A correction factor, obtained through calibration, was then used to convert to actual volume.

2.3.1. Porosity Calculation

The following formulas were used to determine porosity of core plugs: -

$$\text{Pore volume (cc)} = \text{Bulk volume} - \text{Grain volume} \quad [1]$$

$$\text{Porosity (\%)} = \frac{\text{Pore Volume}}{\text{Bulk volume}} \quad [2]$$

$$\text{Grain density (gm/cc)} = \frac{\text{Sample weight}}{\text{Grain volume}} \quad [3]$$

2.4. Nitrogen Gas Permeability

Core plugs were cleaned and dried before being put in the core holder of Hassler-type. The cell was then subjected to 200 psig overburden pressure. One end face of the core plug was subjected to Nitrogen gas pressure and the other end face is subjected to atmospheric pressure. Gas flow was measured at downstream of the core plug. The equipment has a high-pressure precision regulator with a range of 0 to 30 psi at a resolution of 0.01 psi. The equipment's high-pressure transducer range is from 0 to 100 psi, with a resolution of 0.01 psi and accuracy within 0.1%. The low-pressure transducer range is from 0 to 15 psi, with resolution within 0.001 psi, and accuracy within 0.1%.

The following Darcy's equation was used to calculate gas permeability:

$$K_g = \frac{2000 * P_b * Q_g * \mu_g * L}{(P_1^2 - P_2^2) * A} \quad [4]$$

Where K_g is gas permeability in mD, P_b is Barometric pressure in atm, P_1 is Upstream pressure in atm, P_2 is Downstream pressure in atm, Q_g is gas flow rate, cc/sec, μ_g is gas viscosity in cp, L is core plug length in cm and A is the cross-sectional area in sq. cm.

2.5. Klinkenberg Permeability

Klinkenberg permeability correction was calculated using mathematical relationship between K_g and K_I as follows:

$$K_I = 0.68 (K_g)^{1.06} \dots \dots \dots \text{(Empirical Correction)} \quad [5]$$

Core plug liquid permeabilities of the present study varied from 0.5 to 141 mD.

2.6. Porous-Plate Method for Air-Brine Capillary Pressure

Six and nine core plugs were selected from wells A and B, respectively, to perform air-brine capillary pressure measurements. The core plugs were fully saturated and put in a semi-permeable porous diaphragm. Brine volume extracted at controlled pressure of 1, 2, 4, 8, 15, 35, 60, and 120 psi was monitored. The air-brine capillary pressure was converted to oil-brine capillary pressure utilizing air-water and oil-water contact angles of 0 and 30, respectively, and interfacial tension of 72 and 48 dyne/cm, respectively.

3. Results and Discussion

Figs. (5 and 6) illustrate a cross-plot of laboratory-measured porosity and Klinkenberg-corrected permeability on semi-logarithmic plot for core plugs extracted from wells A and B, respectively. The figures also show the developed empirical correlations between porosity and permeability.

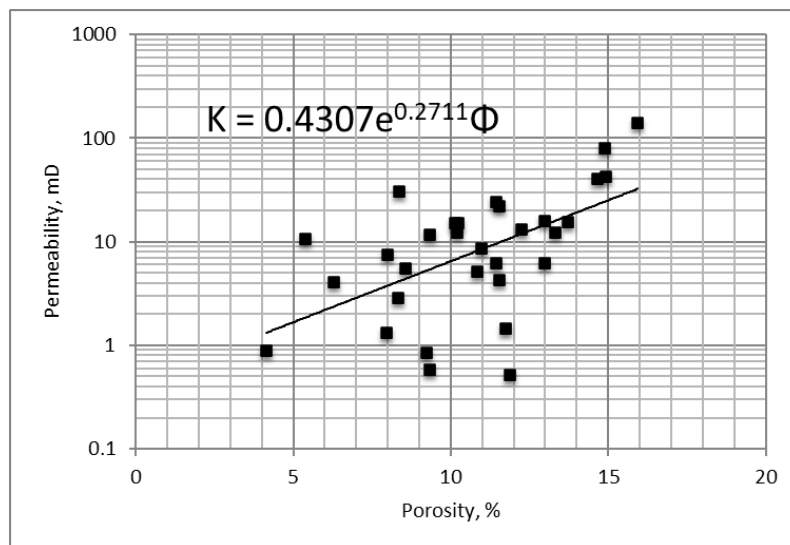


Figure 5: Porosity vs. permeability on a semi-logarithmic scale of core plugs extracted from well A.

There are good correlations between porosity and permeability among the core plugs of the two wells. For core plugs extracted from well A, data are clustered and there is a somewhat good correlation between porosity and permeability. For core plugs extracted from well B, however, permeability increases with porosity; a clearer trend can be observed and a good correlation can be drawn. Unlike the observations from Fig. (5), Fig. (6) shows that permeability deviations from porosity are largely consistent throughout the porosity range. Porosity is primarily determined by pore bodies, thus, rock pore structure measures pore throat size distribution but is independent of porosity. Overall, higher porosity rocks, as unconsolidated sands, are usually associated with uniform pore structure. The less evident correlation between porosity and permeability in Fig. (5) is due to the mostly fractured and vuggy core plugs of well A. Fractured and vuggy porosity does not correlate with permeability [10] as porous media has a narrow pore throat size distribution where mainly the fractures and a few pore throats control most of the porosity. The degree of cementation, sorting, and packing may also influence the relationship between porosity and permeability [4]. Moreover, because threshold pressure controls permeability, the smaller

pore throat effect on permeability is finite. Fig. (5) also shows that porosity and permeability data scatter at lower porosity range and cluster at higher porosity values. Similar observations were also reported by Niya and Selvadurai [1].

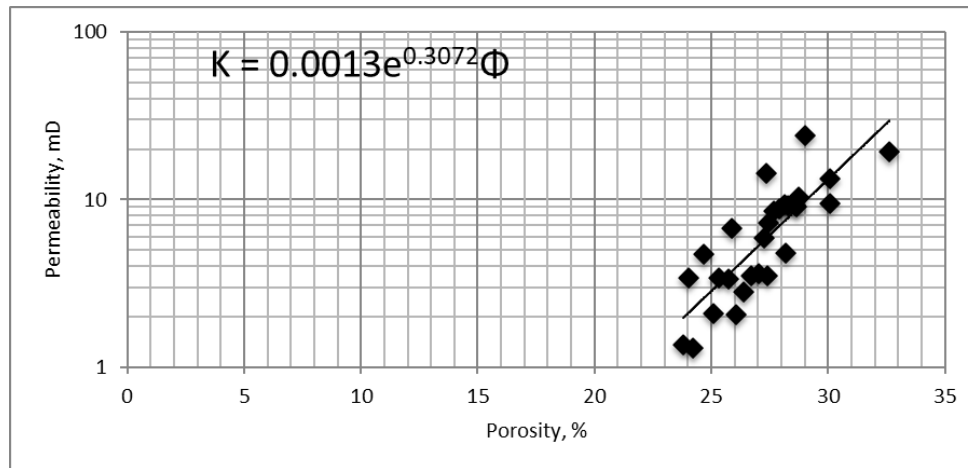


Figure 6: Porosity vs. permeability on semi-logarithmic scale for core plugs extracted from well B.

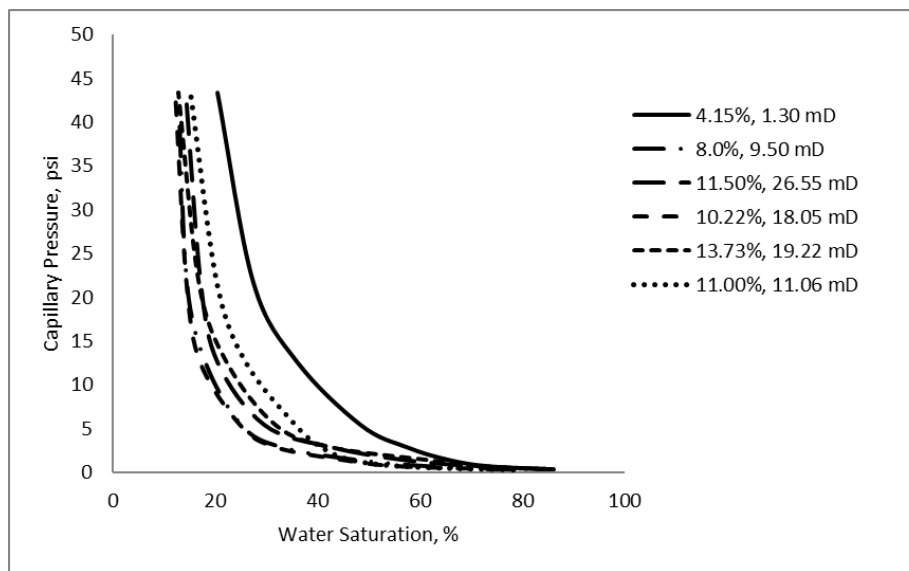


Figure 7: Capillary pressure vs. water saturation of core plugs extracted from well A.

Fig. (7 and 8) illustrate the capillary pressure versus water saturation curves for core plugs extracted from wells A and B, respectively. Both figures show variations in capillary pressure curves for all core plugs as displacement pressure ranges from 0.361 to 43.33 psi. Due to the tortuous and complex pore structure of the core plugs; the overall shape of each capillary pressure curve varies with pore geometry, sorting, and interconnection of the pores within the core plug [21]. Pore size distribution can be independent of pore geometry, however, it differs among the core plugs including those obtained from the same well. Fig. (7) shows that core plugs have more interconnected pore bodies as the plateau region of capillary pressure curves is extended. On the contrary, a steeper slope of the capillary pressure curves is exhibited by the core plugs of well B in Fig (8). Utilizing Purcell [11] method to predict permeability, a deviated computed capillary pressure affects the parameters used to estimate interconnected pore volume leading to inaccurate permeability prediction. Permeability is proportional to the square of pore throat size. Thus, the larger connected throats are much more important than the smaller ones in determining permeability. The contribution of the largest pore throats to permeability is inversely proportional to the threshold pressure. As the non-wetting phase (air) displaces the wetting phase (water) within the core plug, it

preferentially occupies larger interconnected pore bodies because of their small entry threshold pressure. From Fig. (7 and 8), this occurs at capillary pressure of around 5 and 10 psi, respectively. Measured values obtained for the capillary entry pressures are mostly inversely proportional to measured permeability. The non-wetting phase then displaces the wetting phase from smaller pore bodies and throats leading to a sharp increase in capillary pressure associated with a small increase in non-wetting saturation. Fig. (7 and 8) also show that higher displacement rates within the cores have higher permeability because higher permeability indicates larger pore throats and larger interconnected pore bodies. Nonetheless, the overall trend shows that capillary pressure is inversely proportional to permeability. Fig. (7 and 8) show that capillary pressure curves vary remarkably for core plugs within the same well. This, in turn, affects the values of parameters utilized to predict permeability such as those of Swanson [12] and Thomeer [21]. Moreover, this indicates that heterogeneity persists within the core plug scale and pore-scale correlations have some finite cut-off length scale [27, 28].

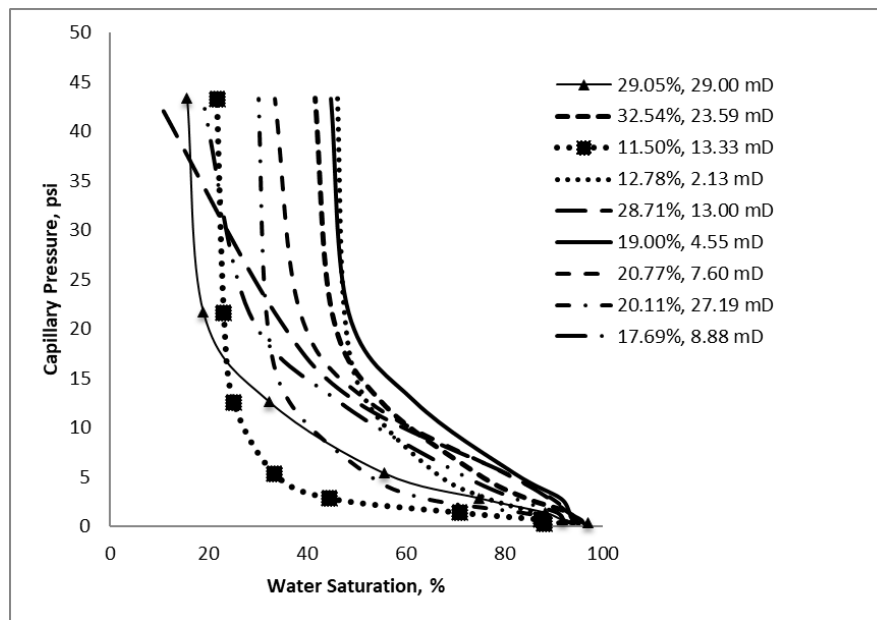


Figure 8: Capillary pressure vs. water saturation of core plugs extracted from well B.

5. Conclusion

Correlations were found and empirical equations were developed between porosity and permeability of sandstone cores. Permeability overall increases as porosity increases. A low degree of correlation was observed for fractured and vuggy core plugs, especially at lower porosity range. Significant variation in capillary pressure curves was observed for core plugs extracted from the same well, however; overall capillary pressure is inversely proportional to permeability.

Conflict of Interest

Authors confirm that there is no conflict of interest.

References

- [1] Niya SMR, Selvadurai APS. A statistical correlation between permeability, porosity, tortuosity and conductance. *Transp Porous Med.* 2018; 121: 741-52. <https://doi.org/10.1007/s11242-017-0983-0>
- [2] Mahmud WM, Yin X, Ermila M. Evaluation of a non-interactive bundle-of-tubes model for calculation of unsteady-state relative permeabilities with laboratory measurements. *J Porous Media.* 2020; 23: 1167-86. <https://doi.org/10.1615/JPorMedia.2020034821>
- [3] Mahmud WM. Rate-controlled mercury injection experiments to characterize pore space geometry of berea sandstone. *E3S Web of Conf.* 2023; 366: Article number 01016. <https://doi.org/10.1051/e3sconf/202336601016>

- [4] Detmer DM. Permeability, porosity, and grain-size distribution of selected pliocene and quaternary sediments in the albuquerque basin. *New Mex Geol.* 1995; 17: 79-87. <https://doi.org/10.58799/NMG-v17n4.79>
- [5] Berg RR. Method for determining permeability from reservoir rock properties. In: Shaw NG, Ed., *Transactions Vol. 20.* Shreveport, Louisiana: Gulf Coast Association of Geological Societies; 1970, pp. 303-17.
- [6] Bloch S. Empirical prediction of porosity and permeability in sandstones. *Am Assoc Pet Geol Bull.* 1991; 75: 1145-60. <https://doi.org/10.1306/20B23C73-170D-11D7-8645000102C1865D>
- [7] Kozeny J. Über kapillare leitung des wassers im boden. *Sitzungsber Akad. Wiss, Wien:* 1927; 136: 271-306.
- [8] Carman PC. Fluid flow through granular beds. *Trans Inst Chem Eng.* 1937; 15: 150-6.
- [9] Mostaghimi P, Blunt MJ, Bijeljic B. Computations of absolute permeability on micro-CT images. *Math Geosci.* 2013; 45: 103-25. <https://doi.org/10.1007/s11004-012-9431-4>
- [10] Ma S, Morrow N. Relationships between porosity and permeability for porous rocks. *International Symposium of the Society of Core Analysts* September 8-10, Montpellier, France: 1996, Paper number 9610.
- [11] Purcell WR. Capillary pressures-Their measurement using mercury and the calculation of permeability. *Trans AIME.* 1949; 186: 39-48. <https://doi.org/10.2118/949039-G>
- [12] Swanson BF. A simple correlation between permeabilities and mercury capillary pressures. *JPT* 1981; 33: 2498-504. <https://doi.org/10.2118/8234-PA>
- [13] Wells JD, Amaefule JO. Capillary pressure and permeability relationships in tight gas sands. *SPE/DOE Low Permeability Gas Reservoirs Symposium* May 19-22, Denver, Colorado: 1985, SPE-13879-MS. <https://doi.org/10.2118/13879-MS>
- [14] Katz AJ, Thompson AH. Quantitative prediction of permeability in porous rock. *Phys Rev B.* 1986; 34: 8179-81. <https://doi.org/10.1103/PhysRevB.34.8179>
- [15] Katz AJ, Thompson AH. Prediction of rock electrical conductivity from mercury injection measurements. *J Geophys Res.* 1987; 92: 599-607. <https://doi.org/10.1029/JB092iB01p00599>
- [16] Thompson AH, Raschke RA, Katz AJ. Estimation of absolute permeability from capillary pressure measurements. *SPE Annual Technical Conference and Exhibition* September 27-30, Dallas: SPE; 1987, p. 27-30. <https://doi.org/10.2118/16794-MS>
- [17] Pittman ED. Relationship of porosity and permeability to various parameters derived from mercury injection-capillary pressure curves for sandstone. *Am Assoc Pet Geol Bull.* 1992; 76: 191-8. <https://doi.org/10.1306/BDFF87A4-1718-11D7-8645000102C1865D>
- [18] Kamath J. Evaluation of accuracy of estimating air permeability from mercury- injection data. *SPE Form Eval.* 1992; 7: 304-10. <https://doi.org/10.2118/18181-PA>
- [19] Huet CC, Rushing JA, Newsham KE, Blasingame TA. A modified purcell/burdine model for estimating absolute permeability from mercury-injection capillary pressure data. *International Petroleum Technology Conference* November 21-23, Doha, Qatar: 2005. p. 21-3. <https://doi.org/10.2523/IPTC-10994-MS>
- [20] Dastidar R, Sondergeld CH, Rai CS. An improved empirical permeability estimator from mercury injection for tight clastic rocks. *Petrophysics.* 2007; 48(3): 186-90.
- [21] Thomeer JHM. Introduction of a pore geometrical factor defined by the capillary pressure curve. *JPT.* 1960; 12: 73-7. <https://doi.org/10.2118/1324-G>
- [22] Dullien F AL. *Porous media: fluid transport and pore structure.* 2nd ed. Academic Press; 2012.
- [23] Serra OE. *Fundamentals of well-log interpretation.* Elsevier; 1983.
- [24] Pittman EdwardD. Relationship of porosity and permeability to various parameters derived from mercury injection-capillary pressure curves for sandstone. *Am Assoc Pet Geol Bull.* 1992; 76: 191-8. <https://doi.org/10.1306/BDFF87A4-1718-11D7-8645000102C1865D>
- [25] Rezaee, MR, Lemon N. Permeability estimation from mercury injection capillary pressure data, a case study in the Tirrawarra Sandstone, Cooper Basin. *Aust Pet Prod Explor Assocn J.* 1997; 37: 824-834.
- [26] Mahmud WM, Bennour Z. Case study of petrophysical evaluation utilizing well logs data with optimization of reservoir cut-off parameters. *Int J Petrol Technol.* 2020; 7: 45-59. <https://doi.org/10.15377/2409-787x.2020.07.5>
- [27] Mahmud WM. The effect of fluid saturation profiles on three-phase oil relative permeabilities and oil recovery. *SPE Annual Technical Conference and Exhibition* November 11-14, Anaheim, California, USA: 2007, SPE-108328-MS. <https://doi.org/10.2118/108328-MS>
- [28] Mahmud WM. Effect of network topology on relative permeability; network model and experimental approaches. *Int J Oil Gas Coal Eng.* 2017; 5: 90-6. <https://doi.org/10.11648/j.ogce.20170505.14>